

Hybrid optical wavelength demultiplexer and power combiner for TWDM PON

CHUNSHENG LI,¹ XINYOU QIU,¹ AND XUN LI^{2,*}

¹Wuhan National Laboratory for Optoelectronics, Huazhong University of Science and Technology, Wuhan 430074, China

²Department of Electrical and Computer Engineering, McMaster University, Hamilton, ON L8S 4K2, Canada

*Corresponding author: lixun@mcmaster.ca

Received 9 December 2016; revised 12 January 2017; accepted 19 January 2017; posted 24 January 2017 (Doc. ID 282534); published 28 February 2017

In this paper, we have proposed a hybrid optical wavelength demultiplexer and power combiner for a hybrid time- and wavelength-division multiplexing (TWDM) passive optical network (PON), i.e., a single passive optical device that functions as a $1 \times N$ wavelength demultiplexer for distributing the downstream signal in multiple wavelengths from the optical line terminal (OLT) to the N optical network units (ONUs), and simultaneously as an $N \times 1$ power combiner for collecting the upstream signal in the same wavelength from the N ONUs to the OLT. Through a design example of a 32 channel hybrid optical wavelength demultiplexer and power combiner on the silicon-on-insulator platform, our numerical simulation result shows that the insertion loss and adjacent channel crosstalk of the downstream wavelength demultiplexer are as low as 4.6 and -16.3 dB, respectively, while the insertion loss and channel non-uniformity of the upstream power combiner can reach 3.5 and 2.1 dB, respectively. The proposed structure can readily be extended to other material platforms such as the silica-based planar lightwave circuit. Its fabrication process is fully compatible with standard clean-room technologies such as photolithography and etching, without any complicated and/or costly approach involved. © 2017 Chinese Laser Press

OCIS codes: (130.3120) Integrated optics devices; (130.7408) Wavelength filtering devices; (230.1360) Beam splitters.

<https://doi.org/10.1364/PRJ.5.000097>

1. INTRODUCTION

With the growing bandwidth demand for Internet and other bandwidth-hungry applications [1], there has been fast development for optical access technologies, such as fiber-to-the-home/curb (FTTH/FTTC) [2,3] networks, to overcome the bandwidth bottleneck. In the conventional time-division multiplexing (TDM) passive optical network (PON) [4], the bandwidth and optical power available to each optical network unit (ONU) are limited due to the splitting loss. Although the wavelength-division multiplexing (WDM) PON can overcome the limitation, in which each ONU is assigned to a specific wavelength, thus enjoying dedicated bandwidth, the high cost has limited its real-world deployment [5,6]. To achieve a proper balance between the performance and cost of PONs, a hybrid TDM/WDM (TWDM) PON [7–10] has been proposed as a promising solution for access networks in which WDM and TDM technologies are separately used for downstream and upstream transmissions, respectively. The asymmetric hybrid TWDM PON in which the download bandwidth is often much greater than the upload bandwidth, is suitable for much more intensive network service, such as high definition television and massive online games. In addition, for upstream transmission, identical low-cost transmitters with their wavelength

set at 1310 nm can be adopted by all ONUs for cost minimizing [11].

As key components in the hybrid TWDM PON, the wavelength demultiplexer [12–14] for downstream transmission and the power combiner [15–17] for upstream transmission have been widely studied. However, the optical module based on multiple discrete components in separated downstream and upstream path design was bulky and not readily scalable with a large number of ONUs [11]. In this work, we have proposed a single passive optical device that can function as a $1 \times N$ wavelength demultiplexer for downstream signal transmission and simultaneously as an $N \times 1$ optical power combiner for upstream signal transmission. The silicon-on-insulator (SOI) waveguide has been chosen as the platform to show the device design idea. The proposed structure can be readily implemented on other material platforms, such as the silica-based planar lightwave circuit (PLC), depending on specific application requirements weighed by multiple factors, including bending and scattering losses, size and uniformity, processing ease, fabrication cost, and production yield. The working principle of the device is described briefly in Section 2. The device design is detailed in Section 3. We then show the numerical simulation results in Section 4, and have our work summarized in Section 5.

2. WORKING PRINCIPLE

To reach the wavelength demultiplexing function for the downstream signal, our proposed structure functions just as a conventional arrayed waveguide grating (AWG). The incident beam with multiple wavelengths propagating through the central input waveguide enters the first free propagation region (FPR) and becomes divergent. The divergent beam is then coupled into the waveguide array and propagates through the individual arrayed waveguides (AWs). As in the conventional AWs, the length difference between adjacent waveguides ΔL is fixed and equal to an integer multiple of the central wavelength λ_0 of the demultiplexer:

$$n_c \Delta L = m \lambda_0, \quad m = 1, 2, 3, \dots, \quad (1)$$

where n_c is the effective index of the AW corresponding to wavelength λ_0 . Through the AWs, light with different wavelength components experiences different phase delays, is consequently focused at different output positions by the diffraction of the second FPR, and is finally collected by different output waveguides.

For the upstream signal, however, the structure would work completely differently from an AWG; rather, it has to become a power (beam) combiner as required.

To explain the working principle of our proposed structure to the upstream signal, we abstract the AWG to a classical dual-lens imaging system, as shown in Fig. 1, where the lens pair 1 and 2 corresponds to the first and second FPR of the AWG, and the object and image focal planes correspond to the planes in which the input and output waveguides of the AWG are placed, respectively. The upstream signal wavelength λ_1 is chosen as

$$\lambda_1 = n'_c \Delta L / m', \quad m' = 1, 2, 3, \dots, \quad (2)$$

where ΔL is the aforementioned adjacent waveguide length difference of the AWs, n'_c is the effective index of the AWs corresponding to wavelength λ_1 , and m' has a different integer value from m . As such, we have ensured that the AWs have no effect on the upstream signal at wavelength λ_1 , as it sees no phase delay at all.

Next, following the relationship between the object–image focal planes, if the input light is launched at a position away from the object focal point on the optical axis (e.g., at point A in Fig. 1), the output light will be focused at a position away from the image focal plane (i.e., at point A' in Fig. 1). Consequently, an expanded spot will be formed on the image

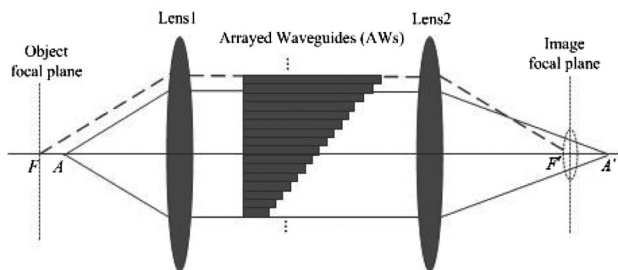


Fig. 1. Schematic diagram for illustration of the proposed structure: while the downstream signal (from F to F') passes through a conventional AWG, the upstream signal (from F' to A) sees an optical power (beam) combiner.

focal plane where the output waveguides are placed for the downstream signal. If the expanded spot size can be designed to match the aperture size of the output waveguide array, an incident beam at a position away from the object focal plane can therefore be coupled into the output waveguides at the image focal plane, and we obtain a power (beam) splitter (at wavelength λ_1). According to optical reciprocity, the upstream signal beams fed into the output waveguides will be combined at the input position by the same structure. Hence, we have a wavelength demultiplexer for the downstream signal at wavelength λ_0 and a power (beam) combiner for the upstream signal at wavelength λ_1 .

3. DEVICE DESIGN

Following the working principle explained above, we have designed a hybrid optical wavelength demultiplexer and power combiner (taking the 32 channel device as an example) on the SOI platform schematically shown in Fig. 2(a). The Si photonic wire with an air cladding is considered in this device, and the cross section is shown in inset 1 of Fig. 2(a). In the x - z plane (top view), the whole device structure is based on a traditional AWG functioning as a wavelength demultiplexer for the downstream signal. However, modifications are introduced to incorporate the combiner design for the upstream signal aiming at not jeopardizing the wavelength demultiplexing performance.

To make our explanation more clear without messing up the input and output waveguides in the device, we will turn the original power combiner for the upstream signal into an equivalent power splitter for the downstream signal at the same wavelength by following optical reciprocity. Hence, the device we are working on can be treated as a wavelength demultiplexer at center wavelength λ_0 and a power splitter at wavelength λ_1 , both for downstream signals with the same input and output ports.

In design of such a device structure, we first need to place the input port for the power splitter in front of that for the wavelength demultiplexer (AWG), according to the working principle of this power splitter (combiner) design explained in Fig. 1. However, a direct implementation of such an idea will need to insert a Si photonic wire inside the first FPR, which apparently wrecks the AWG. To solve this problem, we create a virtual input port for the power splitter by utilizing the beam interference effect, which, instead of inserting a Si photonic wire directly inside the FPR, allows us to place a pair of input Si photonic wires aside the FPR, without blocking the optical path of the AWG, as shown in Fig. 2(a). Following this arrangement, the input light for beam splitting (at wavelength λ_1) will form a conventional bright–dark interference pattern at the exit of the first FPR, as shown in inset 3 of Fig. 2(b), which is then aligned to the discrete AWs with each interference fringe fitted into one AW. By noticing that the phase shift between adjacent fringes is π , we will have to modify the phase condition given in above Eq. (2),

$$\lambda_1 = n'_c \Delta L / (m' + 0.5), \quad m' = 1, 2, 3, \dots, \quad (3)$$

to ensure that all fringes will be in phase after passing through the AWs, as required by the recombining and realigning of the fringes from the AWs to the output waveguides by the second FPR. The insertion position of the input port for the power splitter at the

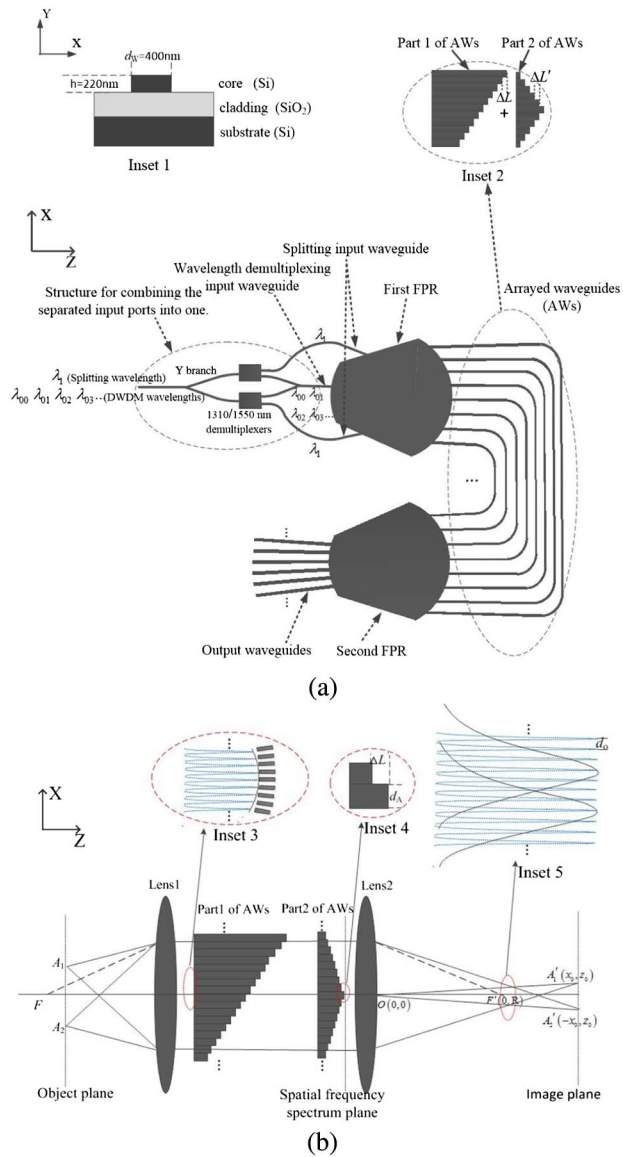


Fig. 2. (a) Schematic (top) view of the hybrid optical wavelength demultiplexer and power combiner; inset 1, cross-sectional view of the Si photonic wire; inset 2, a schematic (top) view of the equivalent AWs and the modifications. (b) Illustration of the proposed structure (excluding the structure for combining the separated input ports into one): while the downstream signal (from F to F') passes through a conventional AWG, the upstream signal (from F' to A_1/A_2) sees an optical power (beam) combiner; inset 3, field distribution with an interference pattern at the input port of the AWs for the upstream signal; inset 4, a zoomed-in view of part 2 of the AWs, where $\Delta L'$ and d_A are the equivalent unit length difference and unit width, respectively; inset 5, interference fringes at the output channels for the upstream signal, where d_O is the interference fringe gap matching to the gap between the output waveguides.

two symmetrical edges of the first FPR needs to be fine tuned for an exact matching between the period of the interference fringes and the separation of the AWs, which appears to be critical in reducing the insertion loss of the splitter (combiner) [18].

Second, the expanded spot at the image focal plane has its intensity following a Gaussian distribution along the lateral

direction (x), rather than a uniform distribution as required by an ideal splitter. To reduce the splitting non-uniformity among output channels, we have added an extra phase delay section to the conventional AWs, shown as part 2 and part 1, respectively, in inset 2 of Fig. 2(a). As shown by the drawing, the extra phase delay section (part 2) is actually a discrete prism that divides one beam into two equal portions. As such, the required interference fringes are formed in the image focal plane with their envelope flattened as a result of the superposition between the two offset Gaussian distributions. This effect is further illustrated in Fig. 2(b). The discrete prism still has to be designed in such a way that the period of its introduced interference fringes will match with the separation of the output waveguides. Actually, the top half part of the prism with its equivalent unit width d_A and unit length difference $\Delta L'$, shown in inset 4 of Fig. 2(b), introduces a linear phase delay $2\pi n'_c \Delta L' x / \lambda_1 d_A$ to a point $(x, 0)$ in the exit plane of the prism ($z = 0$), which also stands as the incident plane of lens 2. Consequently, it generates a corresponding spatial frequency shift $f_x = n'_c \Delta L' / \lambda_1 d_A$ at $(0, R)$ in the focal plane ($z = R$) of lens 2. Its image point $(-x_0, z_0)$ in the image plane must take the same spatial frequency and, thus, have its coordinates given by

$$x_0/z_0 = n'_c \Delta L' / n'_s d_A. \quad (4)$$

The same analysis applies to the bottom half of the prism, and we will have a symmetrical image point (x_0, z_0) generated by a symmetrical point $(-x, 0)$ in the exit plane of the prism. The pair of image points in the image plane, as indicated by A'_1 and A'_2 in Fig. 2(b), will generate an interference pattern with its fringe gap given by

$$d_O = \lambda_1 (z_0 - R) / (2n'_s x_0), \quad (5)$$

matching to the gap between the output waveguides. By eliminating x_0 that corresponds to an arbitrarily selected point x in the exit plane of the prism through Eq. (4), we find

$$d_O = \frac{\lambda_1 d_A (z_0 - R)}{2n'_c z_0} \cdot \frac{1}{\Delta L'}, \quad (6)$$

which links the prism's design parameters (d_A and $\Delta L'$) to the output waveguide gap (d_O) in the image focal plane as required.

Moreover, the extra phase delay brought in by the prism must have minimum effect on the AWG designed as the wavelength demultiplexer for the downstream signal. The length difference $\Delta L'$ of the discrete prism is therefore chosen as

$$\Delta L' = m'' \lambda_0 / n'_c, \quad m'' = 1, 2, 3, \dots, \quad (7)$$

so that the center wavelength component of the downstream signal experiences no extra phase delay at all, when passing through the inserted discrete prism.

Finally, we need to combine the separated input waveguides for the wavelength demultiplexer and power splitter into one general port, to form an in-line bi-directional device with 1-to- N (downstream) and N -to-1 (upstream) ports, as required in the application of the hybrid TWDM PON. For this purpose, shown in Fig. 2(a), two 1310/1550 nm demultiplexers [19] for separating the downstream and upstream signal wavelengths in cascade with a pair of conventional 1-to-2 and 2-to-1 Y-branch combiners are employed.

4. NUMERICAL SIMULATION

We have further employed the wide angle beam propagation method [20,21] to optimize the structural parameters of our proposed design. A set of the final design parameters for the whole device structure is summarized in Table 1, which is optimized for the downstream signal with its central wavelength at $\lambda_0 = 1555.8$ nm and with a wavelength spacing of $\Delta\lambda = 0.8$ nm as defined by the International Telecommunication Union (ITU-T) DWDM grids, and for the upstream signal at wavelength $\lambda_1 = 1303.3$ nm.

With these parameters, the electric field patterns in the first and second FPR are given in Fig. 3, and the simulated device performance is shown in Fig. 4, wherein Figs. 4(a) and 4(b) show the spectral response of the wavelength demultiplexer and the field distribution at the output channels of the power splitter, respectively. For the wavelength demultiplexer, the insertion loss and adjacent channel crosstalk are as low as 4.6 and -16.3 dB, respectively, whereas for the power combiner, the insertion loss and channel non-uniformity are 3.5 and 2.1 dB, respectively. It can also be found in Fig. 4(a) that the insertion loss and adjacent crosstalk of the edge channels in the wavelength demultiplexer are higher than that of the central channel, which is consistent with the design following Eq. (7), since the extra phase delay brought to AWG by the inserted discrete prism can be exactly canceled only at the center wavelength λ_0 of the downstream signal. For edge channels with their wavelength gradually departing away from λ_0 , the inserted discrete prism jeopardizes the required linear phase delay condition in AWG and, hence, deteriorates their performance.

In fabrication of the device, fluctuations on layer thickness, material refractive index, and etching depth are inevitable. These variations bring in an aggregate change on the effective index of the device (especially to AWs), which can be

Table 1. Material and Structural Parameters of the Device

Material and Structural Parameters	Values
Silicon refractive index for λ_0	3.476
Silicon refractive index for λ'_1	3.503
Silica refractive index for λ_0	1.444
Silica refractive index for λ_1	1.447
Output waveguide number N_O	32
Array waveguide number N_A	95
Output waveguide separation d_O (μm)	1.4
Array waveguide separation d_A (μm)	2.4
Input/Output/array waveguide width d_W (μm)	0.4
Rowland circle diameter D (μm)	168.2
Diffraction order m	23
Free spectral range (FSR) (nm)	30.6
AW length difference (part 1) ΔL (μm)	23.4
AW length difference (part 2) $\Delta L'$ (μm)	1.0
Splitting input waveguide position off demultiplexing input waveguide X (μm)	19.8
Splitting input waveguide position off demultiplexing input waveguide Z (μm)	12.6
Y branch angle ($^\circ$)	2
1310/1550-nm demultiplexers length (μm)	312.0
1310/1550-nm demultiplexers width (μm)	3.2
Estimated whole device chip size (μm^2)	900×2500

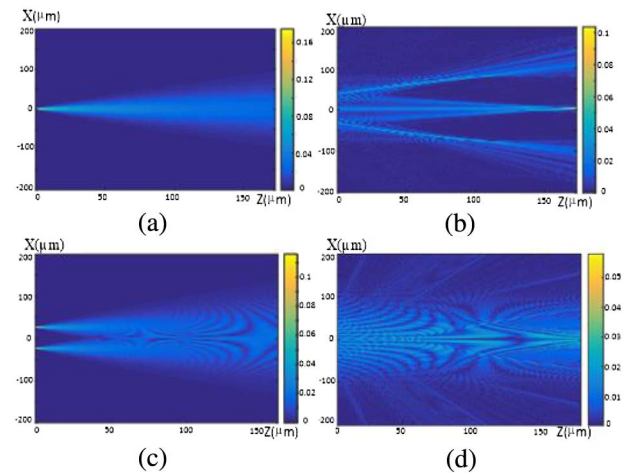


Fig. 3. Electric field patterns in the (a) first FPR and (b) second FPR for the downstream signal at center wavelength λ_0 when the device is working as a wavelength demultiplexer, and electric field patterns in the (c) first FPR and (d) second FPR for the upstream signal when the device is working as a power combiner.

equivalently viewed as a phase noise to AWs that deteriorates the device performance. To mimic this effect, we have added a random phase fluctuation to AWs and simulated the device performance. The random fluctuation is assumed to take a zero-mean Gaussian distribution with a square root variance of 0.25 rad.

The simulated spectral response of channels 23 to 27 in the wavelength demultiplexer for the downstream signal is shown in Fig. 5. We find that, taking the 25th channel as an example,

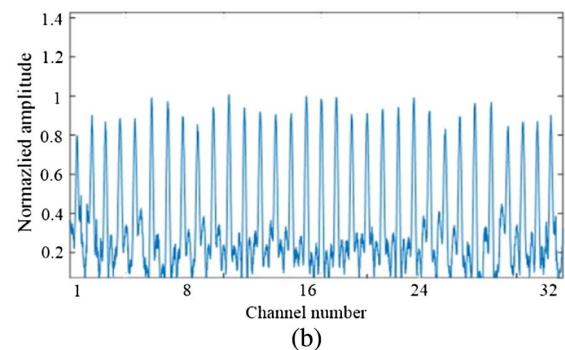
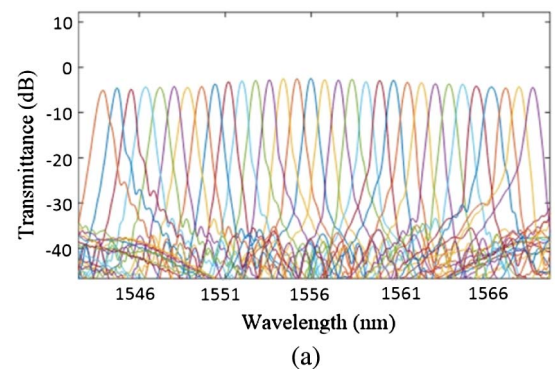


Fig. 4. (a) Spectral response of the downstream wavelength demultiplexer and (b) the field distribution at output channels for the upstream optical power combiner at wavelength $\lambda_1 = 1303.3$ nm.

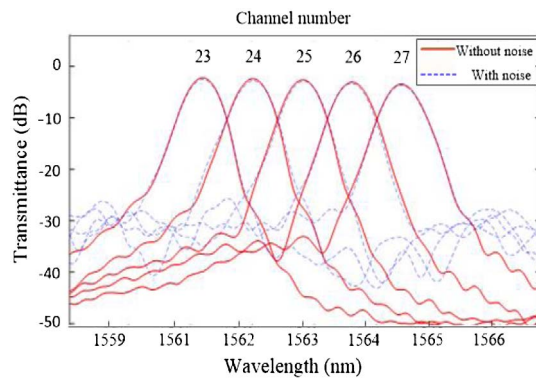


Fig. 5. Spectral response of channels 23 to 27 (with noise) in the wavelength demultiplexer for the downstream signal.

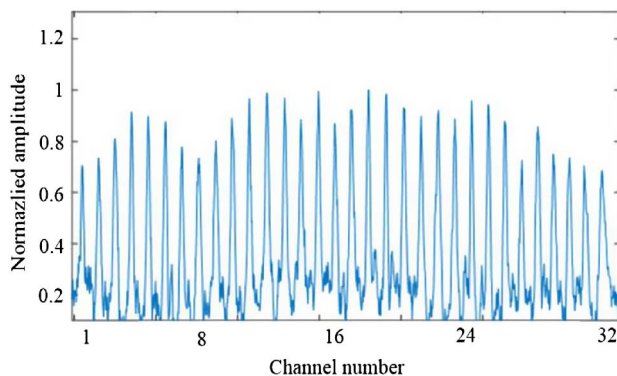


Fig. 6. Field distribution (with noise) at the output channels of the upstream optical power combiner at wavelength $\lambda_1 = 1303.3$ nm.

the insertion loss increases from 3.2 dB (without noise) to 3.4 dB (with noise), the adjacent channel crosstalk increases from -21.8 dB (without noise) to -20.7 dB (with noise), and the non-adjacent channel crosstalk increases from -33.8 dB (without noise) to -25.5 dB (with noise). This result indicates that the phase noise brings in no significant impact on the insertion loss and the adjacent channel crosstalk. However, the phase noise greatly prompts the non-adjacent channel crosstalk.

The simulated field distribution (with noise) at the output channels of the upstream optical power combiner at wavelength $\lambda_1 = 1303.3$ nm are given in Fig. 6. We find that the insertion loss increases from 3.5 dB (without noise) to 4.1 dB (with noise), and the channel non-uniformity increases from 2.1 dB (without noise) to 2.8 dB (with noise). This result indicates that the phase noises bring in a moderate impact on the insertion loss and channel non-uniformity.

To meet with a given requirement on channel crosstalk, channel non-uniformity, and insertion loss, precise control of the structural uniformity in device fabrication is crucial.

5. CONCLUSION

We have proposed, designed, and simulated a hybrid optical wavelength demultiplexer and power combiner. Through a design

example of such a device with 32 channels on the SOI platform, our numerical simulation result shows that the insertion loss and adjacent channel crosstalk of the downstream wavelength demultiplexer are as low as 4.6 and -16.3 dB, respectively, while the insertion loss and channel non-uniformity of the upstream power combiner can reach 3.5 and 2.1 dB, respectively. The proposed device structure can readily be extended to other material platforms such as the silica-based PLC. Its fabrication process is fully compatible with standard clean-room technologies such as photo-lithography and etching, without any complicated and/or costly approach involved. It is worth mentioning that this structure works only for TM-polarized light, and the edge reflection effect in the structure is not considered in our design and simulation. These problems will be tackled in our future work.

REFERENCES

1. R. W. Heron, T. Pfeiffer, D. T. van Veen, J. Smith, and S. S. Patel, "Technology innovations and architecture solutions for the next-generation optical access network," *Bell Labs Tech. J.* **13**, 163–181 (2008).
2. P. W. Shumate, "Fiber-to-the-home: 1977–2007," *J. Lightwave Technol.* **26**, 1093–1103 (2008).
3. D. Meis, "FTTH is on the move," in *IEEE Global Telecommunications Conference (GLOBECOM)*, San Francisco, California (2006).
4. G. Kramer and G. Pesavento, "Ethernet passive optical network (EPON): building a next-generation optical access network," *IEEE Commun. Mag.* **40**(2), 66–73 (2002).
5. S. Park, C. Lee, K. Jeong, H. Park, J. Ahn, and K. Song, "Fiber-to-the-home services based on wavelength-division-multiplexing passive optical network," *J. Lightwave Technol.* **22**, 2582–2591 (2004).
6. A. Banerjee, Y. Park, F. Clarke, H. Song, S. Yang, G. Kramer, K. Kim, and B. Mukherjee, "Wavelength-division-multiplexed passive optical network (WDM-PON) technologies for broadband access: a review [Invited]," *J. Opt. Netw.* **4**, 737–758 (2005).
7. A. R. Dhaini, C. M. Assi, and A. Shami, "Dynamic bandwidth allocation schemes in Hybrid TDM/WDM passive optical networks," in *IEEE Consumer Communications and Networking Conference* (2006), Vol. 6, pp. 30–34.
8. Y. Inoue, A. Himeno, K. Moriwaki, and M. Kawachi, "Silica-based arrayed-waveguide grating circuit as optical splitter/router," *Electron. Lett.* **31**, 726–727 (1995).
9. M. Zirngibl, C. R. Doerr, and C. H. Joyner, "Demonstration of a splitter/router based on a chirped waveguide grating router," *IEEE Photon. Technol. Lett.* **10**, 87–89 (1998).
10. Y. P. Li, L. G. Cohen, C. H. Henry, E. J. Laskowski, and M. A. Cappuzzo, "Demonstration and application of a monolithic two-PONs-in-one device," in *European Conference on Optical Communication (ECOC)* (1996), Vol. 2, pp. 123–126.
11. J. Mu, C. Xu, and W. Huang, "An optical power combiner/wavelength demultiplexing module for hybrid WDM FTTX," *Opt. Express* **17**, 4791–4797 (2009).
12. M. K. Smit and C. Van Dam, "PHASAR-based WDM-devices: Principles, design and applications," *IEEE J. Sel. Top. Quantum Electron.* **2**, 236–250 (1996).
13. W. Bogaerts, S. K. Selvaraja, P. Dumon, J. Brouckaert, K. De Vos, D. Van Thourhout, and R. Baets, "Silicon-on-insulator spectral filters fabricated with CMOS technology," *IEEE J. Sel. Top. Quantum Electron.* **16**, 33–44 (2010).
14. D. Dai and S. He, "Novel ultrasmall Si-nanowire-based arrayed-waveguide grating interleaver with spirals," *Opt. Commun.* **281**, 3471–3475 (2008).
15. Y. Sakamaki, T. Saida, M. Tamura, T. Hashimoto, and H. Takahashi, "Low-loss Y-branch waveguides designed by wavefront matching method and their application to a compact 1×32 splitter," *Electron. Lett.* **43**, 217–219 (2007).

16. M. Bouda, J. Van Uffelen, C. Van Dam, and B. H. Verbeek, "Compact 1×16 power splitter based on symmetrical 1×2 MMI splitters," *Electron. Lett.* **30**, 1756–1758 (1994).
17. C. Li, X. Li, X. Qiu, and Y. Xi, "A novel planar waveguide super-multiple-channel optical power splitter," *J. Lightwave Technol.* **33**, 5019–5024 (2015).
18. K. Suzuki, T. Shibata, Y. Inoue, and H. Takahashi, "Reduction in the diffraction loss of an arrayed-waveguide grating by use of an interference fringe between slab and arrayed waveguides," *Opt. Lett.* **30**, 2400–2402 (2005).
19. Y. Shi, S. Anand, and S. He, "A polarization-insensitive 1310/1550-nm demultiplexer based on sandwiched multimode interference waveguides," *IEEE Photon. Technol. Lett.* **19**, 1789–1791 (2007).
20. W. Huang, C. Xu, S. Chu, and S. K. Chaudhuri, "The finite-difference vector beam propagation method: analysis and assessment," *J. Lightwave Technol.* **10**, 295–305 (1992).
21. G. R. Hadley, "Multistep method for wide-angle beam propagation," *Opt. Lett.* **17**, 1743–1745 (1992).